Research Article | Vol. 27, No. 5 | 4 Mar 2019 | OPTICS EXPRESS 7776
Optics EXPRESS

Optical anisotropy of non-perturbative high-order harmonic generation in gapless graphene

Óscar Zurrón-Cifuentes,[1,*] Roberto Boyero-García,[1] Carlos Hernández-García,[1] Antonio Picón,[2] and Luis Plaja[1]

[1] *Grupo de Investigación en Aplicaciones del Láser y Fotónica, Departamento de Física Aplicada, University of Salamanca, Salamanca E-37008, Spain*
[2] *Departamento de Química, Universidad Autónoma de Madrid, Madrid 28049, Spain*
[*] *ozurronci@usal.es*

Abstract: High harmonic generation in atomic or molecular targets stands as a robust mechanism to produce coherent ultrashort pulses with controllable polarization in the extreme-ultraviolet. However, the production of elliptically or circularly-polarized harmonics is not straightforward, demanding complex combinations of elliptically or circularly-polarized drivers, or the use of molecular alignment techniques. Nevertheless, recent studies show the feasibility of high-harmonic generation in solids. In contrast with atoms and molecules, solids are high-density targets and therefore more efficient radiation sources. Among solid targets, 2D materials are of special interest due to their particular electronic structure, which conveys special optical properties. In this paper, we present theoretical calculations that demonstrate an extraordinary complex light-spin conversion in single-layer graphene irradiated at non perturbative intensities. Linearly-polarized drivings result in the emission of elliptically-polarized harmonics, and elliptically-polarized drivings may result in linearly-polarized or ellipticity-reversed harmonics. In addition, we demonstrate the ultrafast temporal modulation of the harmonic ellipticity.

1. Introduction

High-order harmonic generation (HHG) results from the interaction of physical systems with intense electromagnetic radiation and has led to a large number of relevant applications in attosecond science [1]. HHG is based on the dynamics of the unbound electrons rather than in bound-state transitions, as in conventional perturbative photon up-conversion schemes. As a non-perturbative process, HHG has a noticeable feature: the harmonic spectra show a *plateau*-like structure, followed by a steep drop in efficiency beyond certain cut-off frequency [2]. The *plateau* may extend up to thousands of harmonic orders, allowing the generation of coherent extreme ultraviolet (XUV) or even soft x-ray radiation [3].

High-order harmonics have been observed from a wide diversity of materials. For gas-phase systems, HHG arises from ionized electrons pulled away from their parent atoms or molecules and recolliding back as the field reverses its sign. During recollision electrons may recombine, emitting coherent high-energy photons [4, 5]. For a long time, HHG was thought to be restricted to produce linearly polarized harmonics due to the weak rescattering efficiency when driven by circularly polarized IR pulses [6]. However, several techniques have recently succeeded in generating elliptically and circularly polarized harmonics in atomic gases, using rather sophisticated configurations: HHG driven by a two-color counter-rotating circularly polarized field [7–10]; HHG driven by single-color noncollinear counter-rotating beams [11, 12]; HHG in a double gas jet configuration irradiated by orthogonally polarized beams [13]; or by using molecular targets irradiated by ellipticaly and linearly polarized driving pulses [14–17].

#356082 https://doi.org/10.1364/OE.27.007776
Journal © 2019 Received 26 Dec 2018; revised 6 Feb 2019; accepted 19 Feb 2019; published 1 Mar 2019

Optics EXPRESS

Anisotropic molecules have been also demonstrated to produce elliptical-polarized harmonics out of linear-polarized drivings, after being strongly aligned [18].

High density targets, as crystalline solids, have become increasingly interesting due to their higher efficiency in harmonic conversion and the flexible design of target geometries. HHG in solids, however, is limited by photoinduced damage, which restricts the maximum intensity of the driving field. Until recently, only bulk solids were considered for HHG, with energy gaps larger than the driver photons [19]. HHG from finite-gap solids follows a similar process to atoms or molecules, where ionization is replaced by tunnel excitation from the valence to the conduction band at the driving field maxima, and harmonics are radiated upon electron-hole recombination [20].

Modern materials, such as topological insulators and 2D materials, present a wide variety of electronic structure configurations, controlled by manufacturing, that make them interesting candidates for HHG [21, 22]. Specifically, single-layer graphene (SLG) shows a potential due to the presence of degenerate points in the reciprocal space, that convey extraordinary electronic and optical properties. The singular band-structure provides graphene with a strong non-linear optical response [23, 24]. For instance, second and third harmonics have been observed in multilayer graphene [22, 25–27], and harmonics up to the 9th-order in SLG driven by mid-infrared laser pulses have also been reported [28, 29]. In contrast with the finite-gap case, HHG in graphene relies on the excitation of electron-hole pairs at the Dirac points, which is not associated to tunnel excitation [30]. Dirac points at topological-phase boundaries have been also associated to the enhancement of harmonic conversion [31, 32].

It has been reported that HHG in solids is sensitive to the orientation of the electric field relative to the crystal axis [21, 33, 34]. Recent reports revealed also that HHG in graphene is enhanced by elliptically polarized excitations [28, 35, 36], and that circular-polarized harmonics can be obtained from circular-polarized drivers [36, 37]. In this paper we present a detailed theoretical study of the polarization characteristics of the harmonics induced by a few-cycle infrared laser pulse, as a function of the driver polarization parameters. We analyze the ellipticity, tilt angle and intensity of the harmonics when driven by a laser pulse with different polarizations and orientations. Our results demonstrate an extraordinarily complex photon-spin conversion, leading to a rich scenario for harmonic polarization control: optical rotation, tunable polarization and ultrafast transient polarization. Although time-dependent ellipticity has been observed in the response to circularly and elliptically-polarized drivers in atomic systems [12, 38], here we show that this phenomenon is even stronger for SLG.

2. Methods

Single layer graphene is composed of carbon atoms arranged in an 2D-hexagonal honeycomb lattice, with the first Brillouin Zone as shown in Fig. 1(a). According to the standard tight-binding description of SLG within the nearest-neighbor aproximation [39], the out-of-plane atomic p_z orbitals overlap resulting in π-type bands. Taking the energy of the carbon $2p$ orbitals as reference ($\epsilon_{2p} = 0$), the hamiltonian which describes the electron dynamics in the periodic potential of the crystal is a 2×2 matrix of the form

$$H_0 = \begin{pmatrix} 0 & \gamma f(\mathbf{k}) \\ \gamma f^*(\mathbf{k}) & 0 \end{pmatrix} \tag{1}$$

where $\gamma = 2.97$ eV is the hopping integral and $f(\mathbf{k})$ the complex function:

$$f(\mathbf{k}) = e^{-iak_x/\sqrt{3}} \left(1 + 2e^{i\sqrt{3}ak_x/2} \cos \frac{ak_y}{2} \right), \tag{2}$$

being $a = 2.46$ Å the lattice constant. The band structure of SLG is obtained upon diagonalization of H_0, which yields to eigenvalues $E_\pm(\mathbf{k}) = \pm\gamma|f(\mathbf{k})|$. The wave functions of the corresponding eigenstates of the conduction (+) and valence (-) bands can be written as

$$\Phi_\pm(\mathbf{k};\mathbf{r}) = \sqrt{\frac{1}{2}}e^{i\mathbf{k}\cdot\mathbf{r}}\begin{pmatrix}\pm 1\\ e^{-i\phi(\mathbf{k})}\end{pmatrix}, \tag{3}$$

being $\phi(\mathbf{k})$ the argument of the complex function $f(\mathbf{k})$. $E_\pm(\mathbf{k})$ describe the conduction and valence bands of graphene shown in Fig. 1(b). In the reciprocal space, the high-symmetry points K and K' are degenerated at the energy origin (Dirac points). At their vicinity the band dispersion is linear: electrons and holes behave as massless fermions with constant velocity $v_F \simeq 10^6$ m/s. The maximum energy gap, $\simeq 17.8$ eV, occurs at the center of the Brillouin Zone, labeled Γ in Fig. 1(a). We note that, in practical situations, the chemical potential of graphene can be shifted by electrostatic fields or introducing chemicals. If constant fields are applied near the breakdown threshold, energy shifts of few hundred meV (charge density of few 10^{13} electrons per cm^2) are induced. These values of the chemical potential have a small effect in the optical properties of graphene [40]. Note also that the conduction band occupation with chemical potentials of 100 meV is still very low in comparison with the valence band occupation ($> 10^{15}$ electrons per cm^2) and thus, Pauli blocking is not likely to be relevant. As a result of these considerations, we do not expect that chemical potential shifts affect substantially our results.

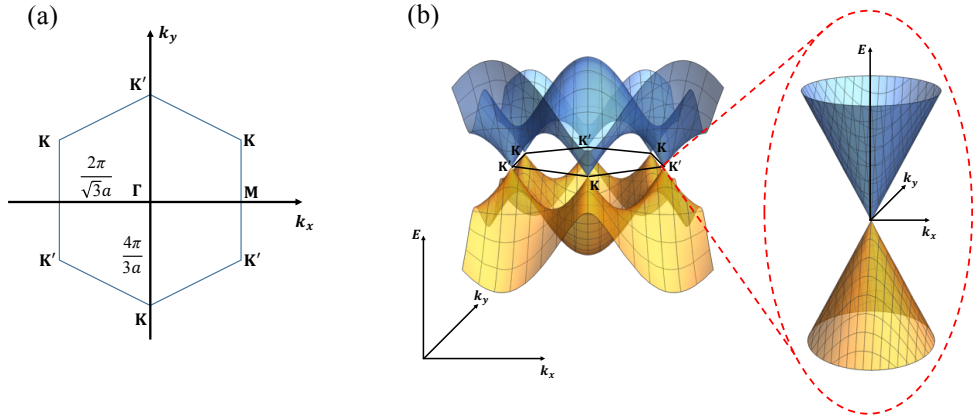

Fig. 1. (a) Scheme of graphene's first Brillouin Zone in the reciprocal space. (b) Graphene's band structure within the nearest-neighbor tight-binding approximation. The Fermi level is set to zero. The conduction and valence bands correspond to positive and negative values of energy, respectively. Dirac points K and K' are degenerated in energy at the Fermi level.

The interaction of the laser pulse $\mathbf{F}(t)$ with the system is described by the time-dependent Hamiltonian $H(t) = H_0 + V_i(t)$, where H_0 is the SLG hamiltonian (1), and $V_i(t) = -q_e\mathbf{F}(t)\cdot\mathbf{r}$ is the electric field coupling in the dipole approximation, being q_e the elementary charge. The time-dependent wave function can be expressed as a superposition of the eigenstates (3):

$$\Psi(\mathbf{r},t) = \int \Psi(\mathbf{k};\mathbf{r},t)d\mathbf{k} = \int \left[C_+(\mathbf{k},t)\Phi_+(\mathbf{k};\mathbf{r}) + C_-(\mathbf{k},t)\Phi_-(\mathbf{k};\mathbf{r})\right] d\mathbf{k}. \tag{4}$$

Following [30], the dynamics can be computed from the integration of the following two-level

Optics EXPRESS

equations at each point of the Brillouin Zone:

$$i\hbar\frac{d}{dt}C^M(\boldsymbol{\kappa}_t,t) = \frac{E_+(\boldsymbol{\kappa}_t)+E_-(\boldsymbol{\kappa}_t)}{2}C^M(\boldsymbol{\kappa}_t,t)+\frac{E_+(\boldsymbol{\kappa}_t)-E_-(\boldsymbol{\kappa}_t)}{2}e^{i\phi(\boldsymbol{\kappa}_t)}\tilde{C}^P(\boldsymbol{\kappa}_t,t) \quad (5)$$

$$i\hbar\frac{d}{dt}\tilde{C}^P(\boldsymbol{\kappa}_t,t) = \frac{E_+(\boldsymbol{\kappa}_t)+E_-(\boldsymbol{\kappa}_t)}{2}\tilde{C}^P(\boldsymbol{\kappa}_t,t)+\frac{E_+(\boldsymbol{\kappa}_t)-E_-(\boldsymbol{\kappa}_t)}{2}e^{-i\phi(\boldsymbol{\kappa}_t)}C^M(\boldsymbol{\kappa}_t,t) \quad (6)$$

where $\hbar\boldsymbol{\kappa}_t = \hbar\mathbf{k} - q_e\mathbf{A}(t)/c$, $\mathbf{A}(t)$ being the vector potential, and

$$C^M(\boldsymbol{\kappa}_t,t) = C_+(\boldsymbol{\kappa}_t,t) - C_-(\boldsymbol{\kappa}_t,t) \quad (7)$$

$$C^P(\boldsymbol{\kappa}_t,t) = e^{-i\phi(\boldsymbol{\kappa}_t)}\left[C_+(\boldsymbol{\kappa}_t,t) + C_-(\boldsymbol{\kappa}_t,t)\right]. \quad (8)$$

We take as initial condition the SLG in its ground state, i.e. $C_-(\mathbf{k},0) = 1$ and $C_+(\mathbf{k},0) = 0$. The harmonic emission is given by the dipole acceleration, i.e. the second time derivative of

$$\mathbf{d}(t) = \langle\Psi(\mathbf{r},t)|q_e\mathbf{r}|\Psi(\mathbf{r},t)\rangle = i\frac{q_e}{2}\int\left[C^{M*}\nabla_{\boldsymbol{\kappa}_t}C^M + C^{P*}\nabla_{\boldsymbol{\kappa}_t}C^P\right]d\mathbf{k}. \quad (9)$$

We have integrated numerically Eqs. (5), (6), and (9), considering an 8-cycle (full extend) driving pulse with $\sin^2$ temporal envelope, modeled as:

$$\mathbf{F}(t) = \sin^2(\pi t/8T)\left[F_x\sin(\omega_0 t)\mathbf{e}_x + F_y\sin(\omega_0 t+\Delta\phi)\mathbf{e}_y\right] \quad (10)$$

where F_x and F_y are the cartesian components of the field amplitude, T is the period, $\omega_0 = 2\pi/T$ the field frequency, and $\Delta\phi$ the relative phase between the field components. We neglect local field corrections to the driving field amplitude, as the field is aimed perpendicularly to the graphene layer and, therefore, propagates through an atomic-size thickness. For the calculations presented in this work, we have considered a wavelength of 3 μm, resulting in a pulse duration of 28 fs (2.9 cycles) at full-width-half-maximum in intensity, ensuring that the pulse length is smaller than the decoherence time due to carrier collisions [41]. We have considered a peak intensity of 5×10^{10} W/cm^2, well below the threshold damage, assuming damage for fluences above 150 mJ/cm^2 [42].

3. Results and discussion

3.1. Linearly polarized laser driver

We first have studied the dependence of the non-linear response of SLG to a linearly-polarized field, i.e. $\Delta\phi = 0$ in Eq. (10), as a function of the tilt angle, $\theta = \arctan(F_x/F_y)$. Figure 2(a) shows the calculated spectra for different values of θ, obtained by the addition of the spectral components $\mathcal{S}_x(\theta,\omega)$ and $\mathcal{S}_y(\theta,\omega)$. The response shows the typical non-perturbative behaviour (*plateau*) up to the seventh harmonic order, followed by a cut-off. These results are in good agreement with the experimental observations reported in [28], where HHG was observed up to the ninth harmonic. As a consequence of the symmetry, the optical response with respect to the driver's polarization follows a periodic pattern with period $\Delta\theta = 60°$. Thus, the harmonic spectrum for $\theta = 30°$ is indistinguible from the one corresponding to $\theta = 90°$ (horizontally polarized driver). Note that the spectra shown in Fig. 2(a) are particularly rich. This is a consequence of the interference of the two different contributions, intraband and interband, as well as of the contributions of different electron-hole pair's trajectories leading to the same harmonic [30].

The fact that the spectra in Fig. 2(a) are not identical demonstrates the anisotropic nature of the optical response of SLG under intense laser fields. As noted previously, anisotropy in HHG is also expected for aligned molecular targets due to the non-spherical symmetry of the molecular orbitals [43]. However, crystalline solids include an additional source of anisotropy, as the dynamics of the electrons in the conduction band are still subjected to the details of the crystal

Optics EXPRESS

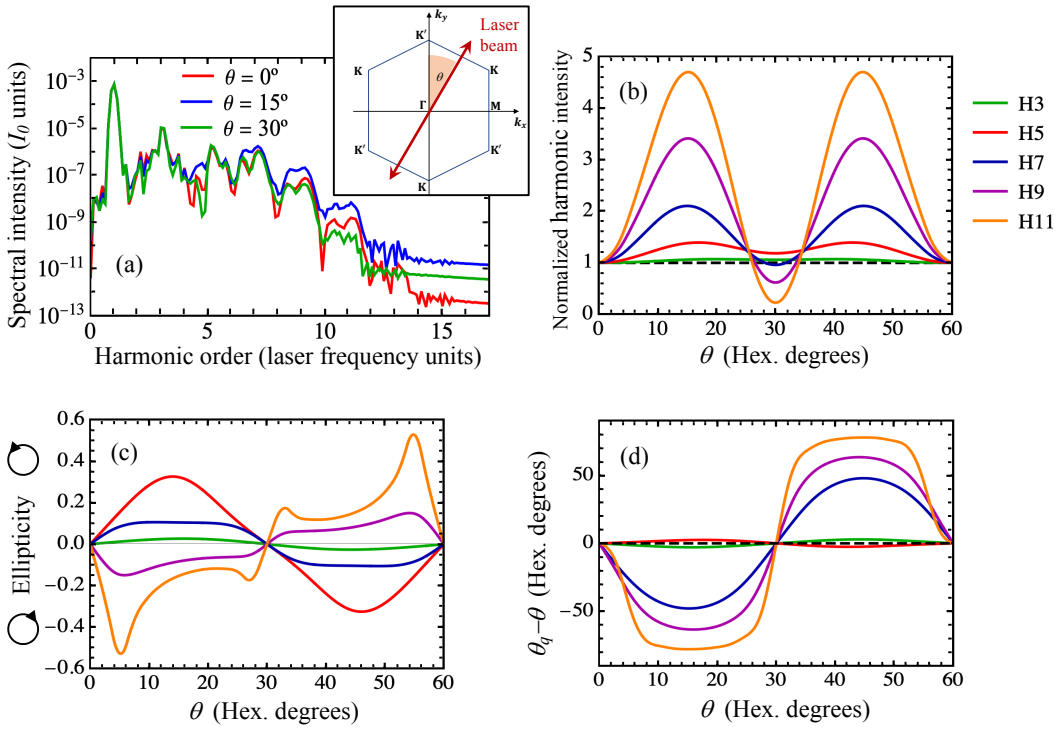

Fig. 2. (a) Total harmonic yield from SLG for different angles of linear polarization of the driving laser, measured from the vertical axis, as shown in the inset. The total yield for each angle is obtained by the addition of the spectral components $\mathcal{S}_x(\theta,\omega)$ and $\mathcal{S}_y(\theta,\omega)$ and it is given in units of the driver's intensity I_0. (b) Intensities of the harmonic yield of SLG as a function of θ. For each harmonic, intensities are normalized to the value at $\theta = 0$. (c) Ellipticity of the harmonic yield as a function of θ. Positive values of the ellipticity indicate left handed polarization. (d) Harmonic tilt angle shift with respect to the driver's tilt, as a function of θ.

potential. In contrast, ionized electrons in molecules behave approximately as free particles and therefore, respond to the field isotropically.

Figure 2(b) shows the variation of the intensity of the harmonic yield with the driver's polarization angle θ. The intensity of each harmonic is normalized to the corresponding value at $\theta = 0$. All the harmonics present a maximum intensity value for $\theta = 15°$ and 45°, which increases with the harmonic order. On the other hand, the harmonic yield finds a minimum efficiency at $\theta = 30°$ for the higher-order harmonics. Note, therefore, that the crystal symmetry axes do not correspond to the optimal driver polarization directions to generate harmonics efficiently.

Figures 2(c) and 2(d) show the dependence of the harmonic ellipticity ε_q and relative tilt angle $\theta_q - \theta$ with respect to the driver's polarization direction. The ellipticity and tilt angle of the q-th harmonic are derived from the Stokes parameters $\{S_0^q, S_1^q, S_2^q, S_3^q\}$, computed from the intensity of the different polarization components, integrated over a spectral window of width ω_0 around

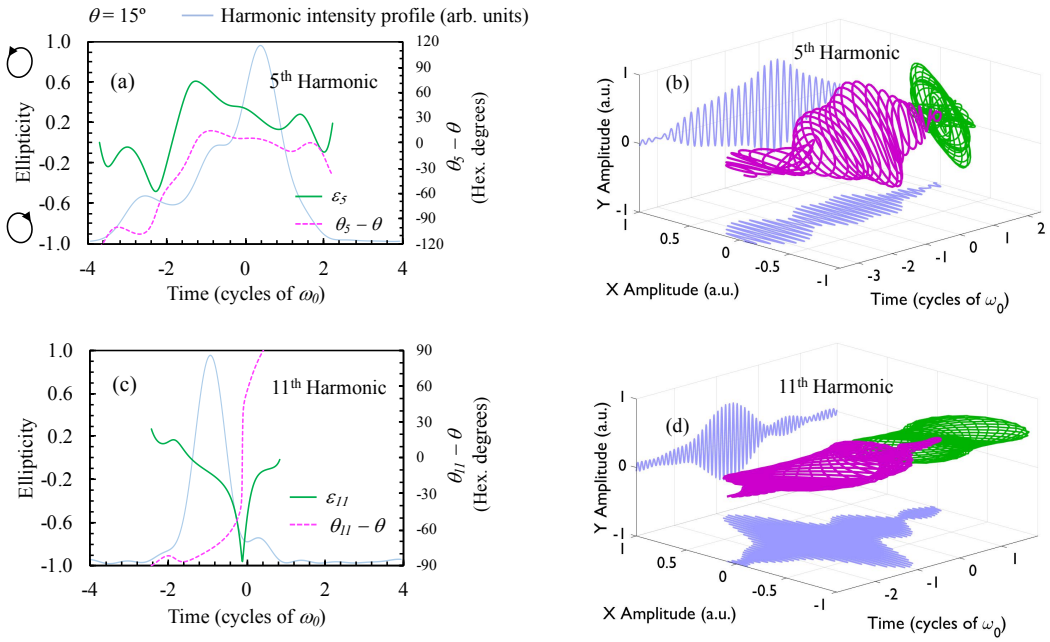

Fig. 3. Time dependent ellipticity for a tilt angle $\theta = 15^\circ$ of the input beam. Panels (a) and (c) show the time dependence of the ellipticity parameter ε_q and relative tilt angle $\theta_q - \theta$ for the fifth and eleventh harmonics, respectively. The blue line in the background of each panel represents the intensity profile of the harmonic emission. Panels (b) and (d) show the 3D plots of the electric field for the fifth and eleventh harmonic pulses along with their ortogonal X and Y components.

each harmonic frequency. Then, the ellipticity and tilt angle are defined as:

$$\varepsilon_q = \tan\left[\frac{1}{2}\arctan\left(\frac{S_3^q}{\sqrt{S_1^{q\,2} + S_2^{q\,2}}}\right)\right], \tag{11}$$

$$\theta_q = \frac{\pi}{2} - \frac{1}{2}\arctan\frac{S_2^q}{S_1^q}. \tag{12}$$

Inspection of Fig. 2(c) reveals that all harmonic orders are linearly polarized when the driving field is aligned with a symmetry axis of the SLG lattice ($\theta = 0$, 30°, etc.), and elliptically polarized elsewhere. The harmonic ellipticity for angles $\theta < 30^\circ$ and $> 30^\circ$ are related by mirror symmetry. We find a remarkable difference between the lower and higher-order harmonics: for angles $\theta < 30^\circ$ the third, fifth and seventh harmonics present left-handed elliptical polarization, whilst the ninth and eleventh are right handed. In contrast, in the case of aligned molecules, the harmonic ellipticity against the driver's tilt behaves similarly for all harmonic orders. According to [20, 30] the frequency of the emitted harmonic corresponds to the instantaneous energy of the electron-hole pair when recombining. This suggests that the third harmonic is generated near the Dirac points, where the band structure is isotropic and therefore, the third-harmonic emission becomes insensitive to the orientation of the driver's polarization.

The combination of the results shown in Figs. 2(b) and 2(c) leaves the conclusion that SLG behaves most efficiently as a source of elliptically polarized harmonics when the driver's

Optics EXPRESS

polarization axis is rotated 15° from the crystal symmetry axes. It also demonstrates that the ellipticity of the harmonics generated in SLG can be easily tuned by changing the tilt angle of the linearly polarized driver, without the need of complex driving configurations.

The orientation of the polarization ellipse (i.e. the tilt angle θ_q of its main axis), is analyzed in Fig. 2(d). The major axis is almost parallel to the signal's polarization for the lower harmonics, while it rotates gradually as the harmonic order increases, reaching a maximal angular difference around $\theta = 15°$ and 45°. For these tilt angles, the main axis of the polarization ellipse of the eleventh harmonic is almost perpendicular to the direction of the driver polarization.

We plot in Fig. 3 the time evolution of the polarization of the harmonics generated at a driver's tilt of 15°, which corresponds to the maximum conversion efficiency, see Fig. 2(b). Our computations show a clear evidence of ultrafast polarization changes both in ellipticity, at the scale of 0.2 per cycle, and tilt angle. The time-dependent harmonic ellipticities are also found in collinear [38] and non-collinear [12] schemes in atomic targets. However, we show that the range and rate of ellipticity variation in SLG are considerable higher. As a general trend, the rate of variation is shown to increase with the harmonic order. This suggests possible applications in ultrafast pump-probe transient absorption experiments.

3.2. *Elliptically polarized laser driver*

We have also investigated the variation of the HHG response to changes in the ellipticity of the driving pulse. We consider a right-handed elliptically polarized driving pulse, as described by Eq. (10) with $\Delta\phi = \pi/2$. The ellipticity of the driver is, therefore, $\varepsilon_{IR} = F_x/F_y$. The rest of the driving field's parameters are defined as in the linear case, so that $\varepsilon_{IR} = 0$ corresponds to the (vertical) linearly polarized driver of the preceding section.

Figure 4(a) shows the calculated harmonic yield for different values of ε_{IR}. The spectra also show the non-perturbative characteristics (*plateau* and cut-off) observed for linear polarization in the previous section. A main observation from Fig. 4(a) is the drop in the efficiency of the HHG for circularly polarized drivings (green line, $\varepsilon_{IR} = 1$). This trend is also observed in atoms, where the number of rescattering trajectories drops drastically with the ellipticity of the driver [44]. However, in comparison with the atomic case, the drop in efficiency in SLG is much weaker. Most interestingly, for $\varepsilon_{IR} = 1$, the three-fold rotational symmetry of graphene forbids the generation of one every three harmonic orders, as it has been recently reported in [36], much in the same way as in atomic HHG driven by two-color counter-rotating fields [7–10].

As a further observation, Fig. 4(a) also shows that the harmonic intensity does not decrease monotonically with the driver's ellipticity, as can be noticed by comparing the red ($\varepsilon_{IR} = 0$) and blue ($\varepsilon_{IR} = 0.3$) curves. We further explore this phenomena in Fig. 4(b), where we plot the normalized harmonic intensity as a function of the driver's ellipticity for different harmonics. The harmonic response is split into two components, parallel to the major axis $\mathcal{S}_y(\varepsilon, \omega)$, dotted lines, and minor axis $\mathcal{S}_x(\varepsilon, \omega)$, solid lines, of the driver's polarization ellipse. All the intesities are normalized by $\mathcal{S}_y$ at $\varepsilon_{IR} = 0$. Note that, while $\mathcal{S}_y$ decreases with the ellipticity for all the harmonic orders, $\mathcal{S}_x$ shows a pronounced increase with a maximum for the driver's ellipticity in the interval $0.3 < \varepsilon_{IR} < 0.4$. This result is in agreement with the experimental data presented in [28]. Complementary, Fig. 4(d) shows the dependence of the ellipticity of each harmonic field as a function of the driver's ellipticity. Note that the region of optimal harmonic conversion in Fig. 4(b) corresponds to harmonics with polarization close to linear. This behavior is the opposite of what we found for the linear-polarized driving in the preceding section, where the optimal conversion efficiency is associated with the generation of elliptically polarized harmonics. Note also that for smaller values of ε_{IR} the polarization is right-handed (as it is the input beam), whilst it turns to left-handed for higher ellipticities. Remarkably enough, for circularly polarized input signal ($\varepsilon_{IR} = 1.0$) the fifth and seventh harmonics are nearly circularly polarized [36], and with opposite handeness, also as found in atomic HHG driven by counter-rotating fields [7–10].

Optics EXPRESS

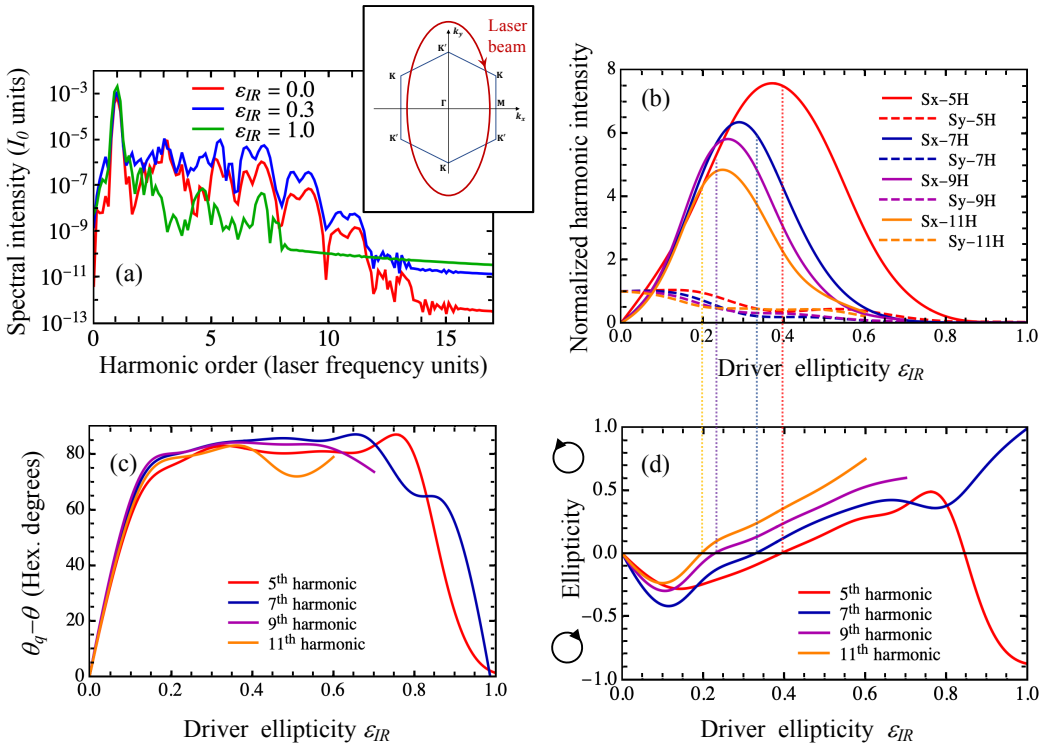

Fig. 4. (a) Harmonic yield from SLG for three different values of the ellipticity of the input beam. The total yield is obtained by the addition of the spectral components $\mathcal{S}_x$ and $\mathcal{S}_y$ parallel to the axes of the laser polarization ellipse and it is given in units of the driver's intensity I_0. (b) Normalized intensities for the harmonic yield as a function of the laser ellipticity. (c) Tilt angle of the harmonic response as a function of ε_{IR}. The tilt angle of the input laser is always zero. (d) Ellipticity of the harmonic yield from SLG as a function of ε_{IR}. Positive values of the ellipticity indicate left handed polarization. The lines connecting graphics (b) and (d) are eye guides. In (b), (c) and (d) the highest harmonics are not plotted for the largest ellipticities because they are not resolved in the spectra.

As additional information, we plot in Fig. 4(c) the tilt angle of the major axis polarization ellipse of each harmonic as a function of the driving field's ellipticity. Our results show that the main axis of the response is almost perpendicular to the main axis of the driving for ellipticity values of maximal efficiency. As shown in Fig. 4(b), this is a consequence of the steep increase of $\mathcal{S}_x$ in these cases. Together with the data shown in Fig. 4(d), we can conclude that the harmonic emission efficiency shows a maximum for driving ellipticities in the range $0.3 < \varepsilon_{IR} < 0.4$, where the harmonics are emitted with polarization close to linear and tilt angles perpendicular to the main axis of the driver's polarization ellipse.

Finally, Fig. 5 shows the time dependent polarization for $\varepsilon_{IR} = 0.3$, i.e. a value corresponding to maximal conversion efficiency according to Fig. 4(b), and for $\varepsilon_{IR} = 1.0$. In the case of the elliptically-polarized drivers, the polarization of the harmonic field varies at the femtosecond scale, in the same way than for linearly-polarized drivings. Note however that the ellipse tilt remains approximately constant at each pulse component of the harmonic field. On the other hand, the ellipticity remains close to pure circular in time when the driving field is circularly-polarized.

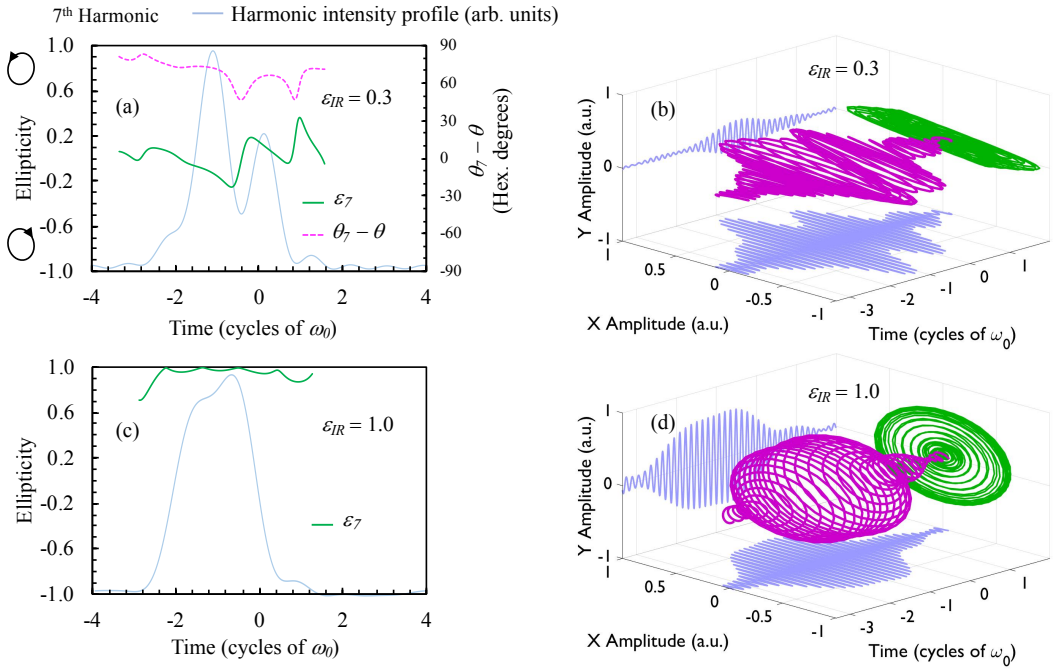

Fig. 5. Panels (a) and (c) show the time dependence of the ellipticity for ε_{IR} = 0.3 and 1.0, respectively. The blue line in the background of each panel represents the intensity profile of the harmonic emission within the laser pulse. Panels (b) and (d) show the 3D plots of the electric field for the harmonic pulses along with its ortogonal X and Y components.

4. Conclusions

We have studied the polarization properties of the high-harmonic emission from single-layer graphene irradiated by intense few-cycle infrared laser pulses with different polarizations. Our numerical results demonstrate that the anisotropic response of SLG induces a complex photon-spin conversion, and thus the production of ellipticaly polarized harmonics from linear-polarized infrared pulses, and linearly polarized harmonics from elliptical-polarized infrared pulses. For the case of elliptically polarized drivers, we have confirmed the increasing role of the polarizability in the x direction, revealing a strong sensitivity of the polarization characteristics of the harmonics field to variations on the driver's ellipticity. Our results also reveal the ultrafast change of the harmonic polarization state, producing pulses with femtosecond time-varying ellipticity. This dynamics may be resolved experimentally using spatial-spectral interferometry [45]. These pulses convey an extraordinary tool for ultrafast pump-probe experiments, ultrafast chiral dichroism [46, 47] and spin/charge dynamics in magnetic materials [48, 49].

Funding

Junta de Castilla y León (SA287P18); Agencia Estatal de Innovación (FIS2016-75652-P, EQC2018-004117-P); Comunidad de Madrid (2017-T1/IND-5432); Agencia Estatal de Investigación (RYC-2017-22745).

References

1. L. Plaja, R. Torres, and A. Zaïr, *Attosecond Physics. Attosecond Measurements and Control of Physical Systems* (Springer-Verlag, 2013).

Optics EXPRESS

2. J. L. Krause, K. J. Schafer, and K. C. Kulander, Phys. Rev. Lett. **68**, 3535-3538 (1992).
3. T. Popmintchev, M. C. Chen, D. Popmintchev, P. Arpin, S. Brown, S. Alisauskas, G. Andriukaitis, T. Balciunas, O. Mücke, A. Pugzlys, A. Baltuska, B. Shim, S. E. Schrauth, A. Gaeta, C. Hernández-García, L. Plaja, A. Becker, A. Jaron-Becker, M. M. Murnane, and H. C. Kapteyn, "Bright Coherent Ultrahigh Harmonics in the keV X-ray Regime from Mid-Infrared Femtosecond Lasers," Science **336**, 1287-1291 (2012).
4. P. B. Corkum, "Plasma perspective on strong field multiphoton ionization," Phys. Rev. Lett. **71**, 1994-1997 (1993).
5. K. J. Schafer, B.Yang, L. F. DiMauro, and K. C. Kulander, "Above threshold ionization beyond the high harmonic cutoff," Phys. Rev. Lett. **70**, 1599-1602 (1993).
6. P. Dietrich, N. H. Burnett, M. Ivanov, P. B. Corkum, "High-harmonic generation and correlated two-electron multiphoton ionization with elliptically polarized light," Phys. Rev. A **50**, R3585-R3588 (1994).
7. D. B. Milosevic, W. Becker, R. Kopold, "Generation of circularly polarized high-order harmonics by two-color coplanar field mixing," Phys. Rev. A **61**, 063403 (2000).
8. A. Fleischer, O. Kfir, T. Diskin, P. Sidorenko, O. Cohen, "Spin angular momentum and tunable polarization in high-harmonic generation," Nat. Photonics **8**, 543-549 (2014).
9. C. Chen, Z. Tao, C. Hernández-García, P. Matyba, A. Carr, R. Knut, O. Kfir, D. Zusin, C. Gentry, P. Grychtol, O. Cohen, L. Plaja, A. Becker, A. Jaron-Becker, H. Kapteyn, M. Murnane, "Tomographic reconstruction of circularly polarized high-harmonic fields: 3D attosecond metrology," Sci. Adv. **2**, e1501333 (2016).
10. K. M. Dorney, L. Rego, N. J. Brooks, J. San-Román, C.T. Liao, J. L. Ellis, D. Zusin, C. Gentry, Q. L. Nguyen, J. M. Shaw, A. Picón, L. Plaja, H. C. Kapteyn, M. M. Murnane, C. Hernández-García, "Controlling the polarization and vortex charge of attosecond high-harmonic beams via simultaneous spin-orbit momentum conservation," Nat. Photonics **13**, 123-130 (2019).
11. D. D. Hickstein, F. J. Dollar, P. Grychtol, J. L. Ellis, R. Knut, C. Hernández-García, D. Zusin, C. Gentry, J. M. Shaw, T. Fan, K. M. Dorney, A. Becker, A. Jaron-Becker, H. C. Kapteyn, M. M. Murnane, C. G. Durfee, "Non-collinear generation of angularly isolated circularly polarized high harmonics," Nat. Photonics **9**, 743-750 (2015).
12. P. C. Huang, C. Hernández-García, J. T. Huang, P. Y. Huang, C. H. Lu, L. Rego, D. D. Hickstein, J. L. Ellis, A. Jaron-Becker, A. Becker, S. D. Yang, C. G. Durfee, L. Plaja, H. C. Kapteyn, M. M. Murnane, A. H. Kung, M. C. Chen "Polarization control of isolated high-harmonic pulses," Nat. Photonics **12**, 349-354 (2018).
13. J. L. Ellis, K. M. Dorney, D. D. Hickstein, N. J. Brooks, C. Gentry, C. Hernández-García, D. Zusin, J. M. Shaw, Q. L. Nguyen, C. A. Mancuso, G. S. M. Jansen, S. Witte, H. C. Kapteyn, M. M. Murnane,"High harmonics with spatially varying ellipticity," Optica **5**, 479-485 (2018).
14. K. J. Yuan, A. D. Bandrauk, "Circularly polarized molecular high-order harmonic generation in H2+ with intense laser pulses and static fields," Phys. Rev. A **83**, 063422 (2011).
15. G. Lambert, B. Vodungbo, J. Gautier, B. Mahieu, V. Malka, S. Sebban, P. Zeitoun, J. Luning, J. Perron, A. Andreev, S. Stremoukhov, F. Ardana-Lamas, A. Dax, C. P. Hauri, A. Sardinha, M. Fajardo "Towards enabling femtosecond helicity-dependent spectroscopy with high-harmonic sources," Nat. Commun. **6**, 6167 (2015).
16. A. Ferré, C. Handschin, M. Dumergue, F. Burgy, A. Comby, D. Descamps, B. Fabre, G. A. Garcia, R. Géneaux, L. Merceron, E. Mével, L. Nahon, S. Petit, B. Pons, D. Staedter, S. Weber, T. Ruchon, V. Blanchet, Y. Mairesse "A table-top ultrashort light source in the extreme ultraviolet for circular dichroism experiments," Nat. Photonics **9**, 93-98 (2015).
17. A. Etches, Ch. B. Madsen, and L. B. Madsen, "Inducing elliptically polarized high-order harmonics from aligned molecules with linearly polarized femtosecond pulses," Phys. Rev. A **81**, 013409 (2010).
18. X. Zhou, R. Lock, N. Wagner, W. Li, H. C. Kapteyn, and M. M. Murnane, "Elliptically Polarized High-Order Harmonic Emission from Molecules in Linearly Polarized Laser Fields," Phys. Rev. Lett. **102**, 073902 (2009).
19. S. Ghimire, A.D. DiChiara, E. Sistrunk, P. Agostini, L.F. DiMauro, and D.A. Reis, "Observation of high-order harmonic generation in a bulk crystal," Nat. Phys. **7**, 138-141 (2011).
20. G. Vampa, C. R. McDonald, G. Orlando, D. D. Klug, P. B. Corkum, and T. Brabec, "Theoretical analysis of High Harmonic Generation in solids," Phys. Rev. Lett. **113**, 073901 (2014).
21. H. Liu, Y. Li, Y.S. You, S. Ghimire, T. F. Heinz, and D. A. Reis, "High-harmonic generation from an atomically thin semiconductor," Nat. Phys. **13**, 262-265 (2017).
22. M. Baudisch, A. Marini, J. D. Cox, T. Zhu, F. Silva, S. Teichmann, M. Massicotte, F. Koppens, L. S. Levitov, F. J. García de Abajo, J. Biegert, "Petahertz optical response in graphene", Nat. Commun. **9**, 1018 (2018)
23. S. A. Mikhailov and K. Ziegler, "Nonlinear electromagnetic response of graphene: frequency multiplication and the self-consistent-field effects," J. Phys.: Condens. Matter **20**, 384204 (2008).
24. K. L. Ishikawa, "Nonlinear Optical Response of Graphene in Time Domain," Phys. Rev. B **82**, 201402 (2010).
25. J. J. Dean and H. M. van Driel, "Second harmonic generation from graphene and graphitic films," Appl. Phys. Lett. **95**, 261910 (2009).
26. N. Kumar, J. Kumar, C. Gerstenkorn, R. Wang, H.Y. Chiu, A.L. Smirl, and H. Zhao, "Third harmonic generation in graphene and few-layer graphite films," Phys. Rev. B **87**, 121406 (2013).
27. S.Y. Hong, J.I. Dadap, N. Petrone, P.C. Yeh, J. Hone, and R.M. Osgood, "Optical Third-Harmonic Generation in Graphene," Phys. Rev. X **3**, 021014 (2013).
28. N. Yoshikawa, T. Tamaya, and K. Tanaka, "High-harmonic generation in graphene enhanced by elliptically polarized light excitation," Science **356**, 736-738 (2017).
29. M. Taucer, T. J. Hammond, P. B. Corkum, G. Vampa, C. Couture, N. Thiré, B. E. Schmidt, F. Légaré, H. Selvi, N.

Optics EXPRESS

Unsuree, B. Hamilton, T. J. Echtermeyer and M. A. Denecke, "Nonperturbative harmonic generation in graphene from intense midinfrared pulsed light," Phys. Rev. B **96**, 195420 (2017).
30. O. Zurrón, A. Picón, and L. Plaja, "Theory of high-order harmonic generation for gapless graphene," New J. Phys. **20** 053033 (2018).
31. A. Chacón, W. Zhu, Sh. P. Kelly, A. Dauphin, E. Pisanty, A. Picón, Ch. Ticknor, M. F. Ciappina, A. Saxena, M. Lewenstein "Observing Topological Phase Transitions with High Harmonic Generation," arXiv:1807.01616 [cond-mat.mes-hall] (2018).
32. R. E. F. Silva, A. Jiménez-Galán, B. Amorim, O. Smirnova, and M. Ivanov, "Topological strong field physics on sub-laser cycle time scale," arXiv:1806.11232v2 [physics.optics] (2018).
33. F. Langer, M. Hohenleutner, C. P. Schmid, C. Poellmann, P. Nagler, T. Korn, C. Schüller, M. S. Sherwin, U. Huttner, J. T. Steiner, S. W. Koch, M. Kira, and R. Huber, "Lightwave-driven quasiparticle collisions on a subcycle timescale," Nature **533**, 225-229 (2016).
34. Y. S. You, J. Lu, E. Cunningham, Ch. Roedel, and S. Ghimire, "Crystal orientation-dependent polarization state of high-order harmonics," arXiv:1810.11567v1 (2018).
35. C. Liu, Y. Zheng, Z. Zeng, and R. Li "Driving-laser ellipticity dependence of high-order harmonic generation in graphene." Phys. Rev. A **97**, 063412 (2018).
36. Z.Y. Chen and R. Qin,"Circularly polarized extreme ultraviolet high harmonic generation in graphene," arXiv:1808.07346v2 (2018).
37. S. A. Sørngård, S. I. Simonsen, and J. P. Hansen, "High-order harmonic generation from graphene: Strong attosecond pulses with arbitrary polarization," Phys. Rev. A **87**, 053803 (2013).
38. L. Barreau, K. Veyrinas, V. Gruson, S. J. Weber, T. Auguste, J. F. Hergott, F. Lepetit, B. Carré, J. C. Houver, D. Dowek, and P. Salières, Pascal, "Evidence of depolarization and ellipticity of high harmonics driven by ultrashort bichromatic circularly polarized fields," Nat. Commun. **9**, 4727 (2018).
39. S. Reich and Ch. Thomsen, and J. Maultzsch, *Carbon Nanotubes: Basic Concepts and Physical Properties* (Wiley-Vch Verlag, 2004).
40. F. Zhou and W. Du, "The graphene Mach-Zehnder modulator based on sandwiched structure," Res J Opt Photonics **2**, 1000110 (2018).
41. M. Breusing, C. Ropers and Th. Elsaesser, "Ultrafast carrier dynamics in graphite," Phys. Rev. Lett. **102** 086809 (2009).
42. A. Roberts, D. Cormode, C. Reynolds, T. Newhouse-Illige, B. J. LeRoy, and A. S. Sandhu, "Response of graphene to femtosecond high-intensity laser irradiation," Appl. Phys. Lett. **99**, 051912 (2011).
43. E. Skantzakis, S. Chatziathanasiou, P. A. Carpeggiani, G. Sansone, A. Nayak, D. Gray, P. Tzallas, D. Charalambidis, E. Hertz and O. Faucher, "Polarization shaping of high-order harmonics in laser-aligned molecules," Scientific Reports **6**, 39295 (2016).
44. K. S. Budil, P. Salières, A. L' Huillier, T. Ditmire, and M. D. Perry, "Influence of ellipticity on harmonic generation,", Phys. Rev. A **48**, R3437-R3440 (1993).
45. M. W. Lin and I. Jovanovic, "Single-Shot Measurement of Temporally-Dependent Polarization State of Femtosecond Pulses by Angle-Multiplexed Spectral-Spatial Interferometry," Scientific Reports **6**, 32839 (2016).
46. R. Cireasa, A. E. Boguslavskiy, B. Pons, M. C. H. Wong, D. Descamps, S. Petit, H. Ruf, N. Thiré, A. Ferré, J. Suarez, J. Higuet, B. E. Schmidt, A. F. Alharbi, F. Légaré, V. Blanchet, B. Fabre, S. Patchkovskii, O. Smirnova, Y. Mairesse, V. R. Bhardwaj. "Probing molecular chirality on a sub-femtosecond timescale," Nat. Phys. **11**, 654-658 (2015).
47. S. Beaulieu, A. Comby, D. Descamps, B. Fabre, G. A. Garcia, R. Géneaux, A. G. Harvey, F. Légaré, Z. Masín, L. Nahon, A. F. Ordonez, S. Petit, B. Pons, Y. Mairesse, O. Smirnova, V. Blanchet, "Photoexcitation circular dichroism in chiral molecule," Nat. Phys. **14**, 484-489 (2018).
48. C. Boeglin, E. Beaurepaire, V. Halté, V. López-Flores, C. Stamm, N. Pontius, H. A. Durr, J.-Y. Bigot, "Distinguishing the ultrafast dynamics of spin and orbital moments in solids," Nature **465**, 458-461 (2010).
49. P. Tengdin, W. You, C. Chen, X. Shi, D. Zusin, Y. Zhang, C. Gentry, A. Blonsky, M. Keller, P. M. Oppeneer, H. C. Kapteyn, Z. Tao, M. M. Murnane, "Critical behavior within 20 fs drives the out-of-equilibrium laser-induced magnetic phase transition in nickel," Sci. Adv. **4**, 9744 (2018).